

# Investigation and Optimization of an Instationary MPD Thruster at IRS

IEPC-2005-208

Presented at the 29<sup>th</sup> International Electric Propulsion Conference, Princeton University, October 31 – November 4, 2005

Anuscheh Nawaz<sup>\*</sup>, Monika Auweter-Kurtz<sup>†</sup>, Georg Herdrich<sup>‡</sup> and Helmut L. Kurtz<sup>§</sup>  
University of Stuttgart, Institut für Raumfahrtsysteme, 70550 Stuttgart, Germany

Motivated by the prospective use on a lunar mission, a pulsed instationary magnetoplasmadynamic thruster is being designed at the Institut für Raumfahrtsysteme (IRS). Two results will be mainly discussed in this paper: The first optimization step of the geometry of the thruster and a thrust balance designed to measure pulsed, low impulse bits. In particular, the width of the electrodes was reduced to successfully raise the efficiency. In addition, first measurements with a vertical pendulum were performed. Evaluation of this data based on the energy balance equation showed results in the order of magnitude expected.

## I. Introduction

At the *Institut für Raumfahrtsysteme* in Stuttgart, Germany, an instationary pulsed magnetoplasmadynamic thruster (I-MPD, also referred to as pulsed plasma thruster, PPT) is being built. This project was initiated when the *Small Satellite Program* was started at IRS in 2002. This program includes the launch of four satellites, developed at this institute. One of the satellites, BW1, is an all electrical satellite bound to the moon<sup>[1]</sup>. Two types of electric thrusters will provide the  $\Delta v$  necessary. One of them is a thermal arcjet with a thrust level of around 100 mN<sup>[2]</sup>; the other is the I-MPD thruster SIMP-LEX (Stuttgart Instationary Magnetoplasmadynamic Thruster for Lunar Exploration). The first will be used for phases that require higher

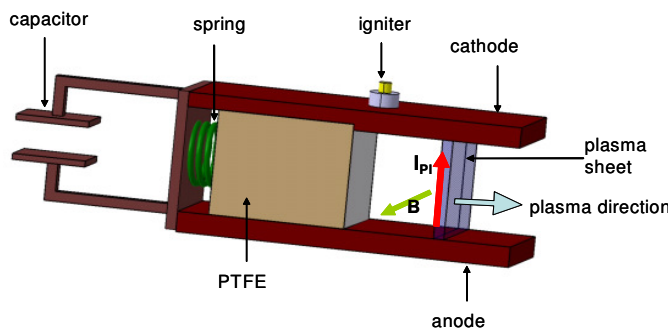


Figure 1. Working Principle of an I-MPD

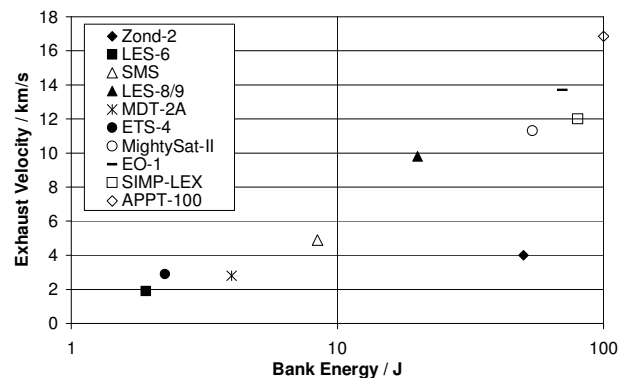


Figure 2. Overview of Exhaust Velocity over Bank Energy for Various I-MPDs<sup>[3,4,5,6]</sup>

<sup>\*</sup> Doctoral Candidate, Institut für Raumfahrtsysteme (IRS), nawaz@irs.uni-stuttgart.de.

<sup>†</sup> Head of the Department of "Space Transportation Technology", Institut für Raumfahrtsysteme (IRS), auweter@irs.uni-stuttgart.de.

<sup>§</sup> Head of Laboratory, Institut für Raumfahrtsysteme (IRS), kurtz@irs.uni-stuttgart.de.

<sup>‡</sup> Senior Researcher, Institut für Raumfahrtsysteme (IRS), herdrich@irs.uni-stuttgart.de.

thrust levels, such as the ascent phase immediately after separation from launcher, elevating the orbit above the Van Allen belt. A cluster of I-MPDs serve as cruise propulsion system. The I-MPD was chosen as cruise thruster because of its simple design, its reliability as well as its capability to easily adjust to different power levels due to its pulsed energy release without loss of performance. On small satellites, power is usually one of the tightest constraints. Although SIMP-LEX is the first I-MPD thruster in Stuttgart, the development of such a thruster at IRS can draw from over 30 years of expertise in the field of electric propulsion.

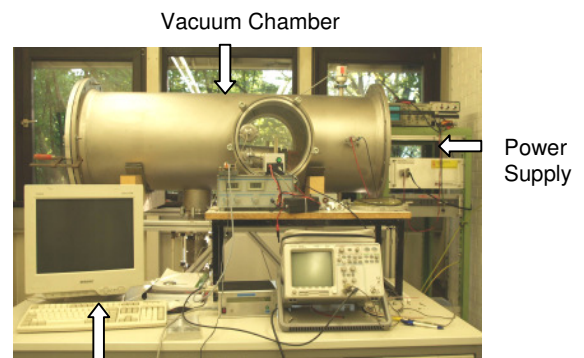
In principle, a parallel plate I-MPD consists of two parallel electrode plates between which a solid propellant block (Polytetrafluorethylen, PTFE) is placed, see Fig.1. The capacitor is charged externally and discharges across the surface of the PTFE, forming PTFE-plasma, once the igniter is fired. An electrical circuit with current  $I_{pl}$  and its own magnetic field  $B$  is formed. Consequently, the plasma is accelerated outwards along the electrodes according to the Lorentz law resulting in an impulse bit on the thruster in the opposite direction.

Figure 2 shows an overview of several I-MPD thrusters. Filled icons indicate the mission was already launched. SIMP-LEX will have a bank energy of around 80 J and its expected exhaust velocity is 12 000 m/s. In order to serve as a cruise propulsion system the cluster of I-MPDs will have to provide a total average thrust of 6 mN.

### A. Test Facility Setup

In its final stage, the test facility for the I-MPD will be comprised of three vacuum chambers: one in which the thrust is measured, one for conducting life expectancy tests, and one for optimizing components and geometry of the thruster. Currently, the first two have been setup, where the facility in which the thrust is measured also serves for geometry and current investigations. It is shown in Fig. 3. The pressure in the vacuum chambers reaches about  $10^{-5}$  mbar prior to firing the thruster.

The electronics providing the voltage to the capacitor as well as the voltage peak to the spark plug was developed by ASP GmbH in Friedrichshafen. Its bread board stage allows for different voltage settings for charging the capacitor as well as various pulse frequencies in the automatic firing mode.



Data Readout at 200MHz  
**Figure 3. One of the I-MPD Test Facilities**

### B. Thruster Setup

The current setup of the I-MPD thruster is shown in the pictures in Fig. 4. It shows its parallel plate geometry, as well as its highly modular setup. This setup allows for easy changes of components and geometry which are currently being optimized. Fig. 4 a) shows the configuration of the capacitor, the copper electrodes and the igniter. The distance  $h$  between the electrodes in Fig. 4 b) can be changed incrementally by using a different set of holes in the red half shell for mounting the electrode plates, as seen in the left picture. The width  $d$  of the electrodes as well as their length can be varied freely. The current values for the thruster can be seen in

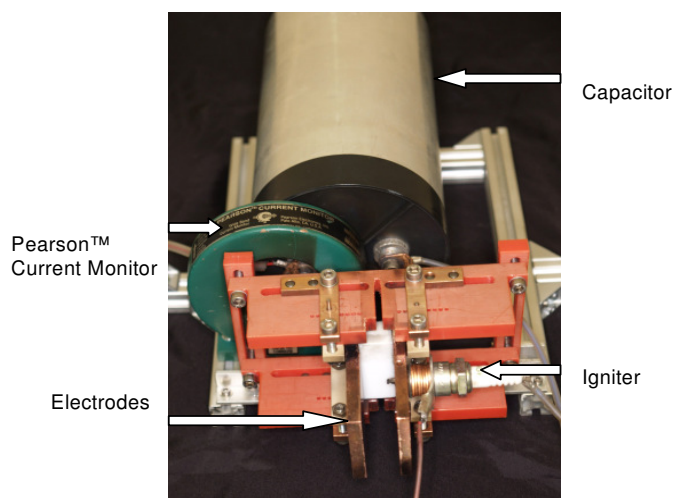


**Figure 4a. Current Setup of SIMP-LEX**

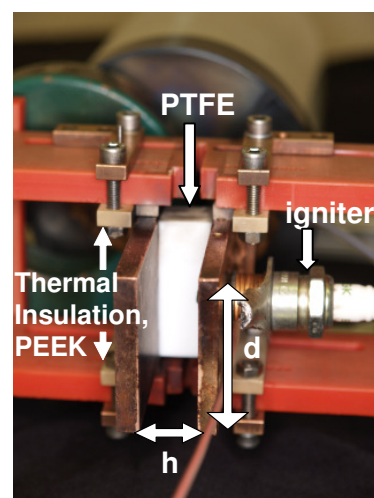


**Figure 4b. Close-Up Front View of SIMP-LEX**

Table 1. However, they are still subject to optimization.  $L$  is the distance the plasma covers from the propellant surface to the end of the electrodes. First tests at a pulse frequency of 1.2 Hz showed that it is necessary to insulate the PE (Polyethylen) half shells (red) thermally from the plasma and the copper electrodes. This was realized by placing PEEK spaceholders between the electrodes and the half shell and by moving the half shell backwards, away from the plasma.

Capacity	1 x 40 $\mu$ F
Maximum Voltage	2200V
h	20 mm
d	40 mm
L	47 mm

**Table 1. Current I-MPD Design Parameters**

### C. Measurement of Plasma Current and Mass Bit Ablated

Figure 4 also shows the Pearson<sup>TM</sup> current monitor, placed between the electrodes and the capacitor. It serves as a Rogowski coil and outputs a voltage proportional to the current through the coil.

The mass bit is measured by comparing the weight of the propellant bar before and after at least 150 pulses. The balance used has a precision of 10  $\mu$ g.

### D. Measurement of Thrust

The thrust is measured by placing the I-MPD on a vertical pendulum as seen in Fig. 5 and determining the deflection caused by the impulse bit through an optical sensor at the bottom of the structure. The pendulum consists of an aluminum frame to which the thruster is fixed by anodized aluminum bars. Two electrically insulated torsion springs serve as suspension. Torsion springs are used to reduce the energy loss to the suspension to zero. In addition, these springs serve as electric feed through to the capacitor. In its final design, this allows for no extra wires leading onto the pendulum, thus resulting in less damping of the movement allowing greater deflection. At present, however, the power supply to the igniter still leads from the igniter to the top of the frame from where it is loosely hung from there to the feed through of the vacuum chamber. These wires are being removed by placing the electric circuit necessary for firing the igniter on the pendulum itself, alongside with batteries to supply the power. The igniter will be triggered optically through one of the windows of the vacuum chamber.

The deflection of the pendulum, caused by one pulse of the thruster is measured by using an optical position encoder consisting of a readhead and a self adhesive scale. The scale is a measurement tape like device. It has gold coated divisions equally spaced at 200  $\mu$ m and is attached to the pendulum. The readhead is placed 0.7 mm away from the pendulum. It consists of an LED and a photodiode and is mounted on a platform welded to the vacuum chamber. When the scale moves relative to the readhead the photodiode detects a change in signal from the LED reflecting off the tape. In order to precisely align the readhead, the position of the pendulum can be adjusted around the x and z axis. Further, the sensor is mounted on a set of micrometer screws, allowing for accurate distance placing in x and y direction. The resolution of the deflection measurement system installed is 50 nm.

The thrust balance will be calibrated using a piezo impulse hammer mounted on a stroke magnet inside the chamber. This will allow for calibrations in between measurements.

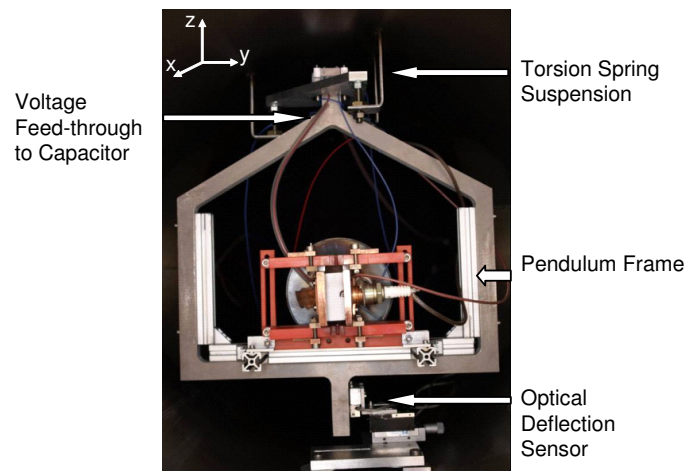


**Figure 5. Thrust Balance with Mounted Thruster**

## II. Methodology

The data received from the oscillation of the pendulum was investigated using the law on conservation of energy and the equation of motion. Further, a first step towards optimizing the thruster was made following investigations conducted with regard to varying the distance  $h$  between the electrodes. Both methodologies will be discussed here.

### A. Thrust Balance

The law of conservation of energy was applied to this problem in order to obtain information on the thrust from the I-MPD. For this rough calculation, the energy  $W_T$  provided from the thruster was assumed to transform

completely into potential energy  $W_H$  and deformation energy  $W_D$  of the torsion spring, evaluated at the point of maximum deflection. Energy loss due to vibration of the pendulum arm itself is neglected. Equation (1) and (2) describe this.

$$W_T = W_H + W_D \quad (1)$$

$$W_T = mgh + \frac{1}{2} D \rho^2 = \frac{1}{2} \bar{M}^2 \frac{T_a^2}{\Theta} \quad (2)$$

The mass  $m$  of the pendulum/thruster system multiplied by the gravity constant  $g$  and the height  $h$  reached at the first point of maximum deflection form the potential energy. The torsion spring constant  $D$  and the angle  $\varphi$  from the vertical reference line are needed to calculate the energy inside the torsion springs. The mean moment  $\bar{M}$  caused by the thruster, the time  $T_a$  during which the plasma is accelerated, and the moment of inertia  $\Theta$  comprise the energy delivered from the I-MPD. To find out the force behind this moment the distance  $l_T$  of the thrust from the rotation axis must be known.

$$\bar{F}^2 = \frac{2\Theta \left( mgh + \frac{1}{2} D \rho^2 \right)}{T_a^2 l_T^2} \quad (3)$$

This force is the average force from the thruster during the time of plasma acceleration.

The moment of inertia  $\Theta$  was determined from the equation of motion as described below. The mass  $m$  was measured using a scale,  $h$  was derived from the deflection measurement according to:

$$h = l_M (1 - \cos \rho), \quad (4)$$

where  $l_M$  is the distance from the axis of the pendulum to the point where the deflection is measured and  $\varphi$  is calculated from the maximum deflection  $x_{\max}$  measured:

$$\rho = \arcsin \left( \frac{x_{\max}}{l_M} \right). \quad (5)$$

The torsion constant  $D$  is provided by the manufacturer.  $T_a$  is taken from the current measurement.

In order to describe the damped oscillatory motion of the pendulum, the equation of motion is derived. The momentum equation for the thrust balance under investigation is:

$$\ddot{\rho} + \frac{R}{\Theta} \dot{\rho} + \frac{(D + mg)}{\Theta} \rho = \frac{M}{\Theta}. \quad (6)$$

Here  $R$  is the damping constant of the oscillation. The term  $(mg\varphi)$  originates from the gravitational force in the direction of motion ( $mg \sin \varphi$ ), where  $\sin \varphi \approx \varphi$  for the small angles reached here. The moment  $M$  from the thruster is zero for time  $t > T_a$ , after the thruster stopped firing. Since the motion of the pendulum during the time the thruster fires is in the order of the resolution of the measurements taken, only the time interval  $t > T_a$  is investigated.

The solution to this differential equation with the moment  $M=0$  is an equation for damped oscillation:

$$x(t) = A e^{\alpha t} \sin(\omega t + \alpha) + c. \quad (7)$$

In this equation,  $x$  is the deflection measured by the sensor described in section I-D.  $A$  is the amplitude of the oscillation,  $\delta$  is the damping factor,  $\omega$  is the angular velocity and  $\alpha$  is the angle the oscillation is shifted from a sinusoidal motion along the  $x$ -axis. The constant  $c$  allows for shifting of the dataset along the  $y$ -axis.

The function specified in Eq.(7) was fit to the data from the deflection sensor varying the parameters  $A$ ,  $\delta$ ,  $\omega$ ,  $\alpha$  and  $c$  by means of a least squares minimization.

The term multiplied by  $\varphi$  is the angular velocity squared. Knowing this, the moment of inertia  $\Theta$  can be determined for the system:

$$\Theta = \frac{(D + mg)}{\omega^2}. \quad (8)$$

The center of mass at the distance  $L_0$  from the rotation axis of the pendulum is derived from that by applying:

$$\Theta = m L_0^2. \quad (9)$$

## B. Thruster Geometry

The geometry and components of SIMP-LEX should be optimized such that a very high specific impulse  $I_{sp}$  is reached at thrust levels around 1 mN. In order to reach this goal the slug model [7] was investigated with respect to  $I_{sp}$ , the impulse caused by one pulse  $I_{bit}$  and the thruster efficiency  $\eta_{el}$ .  $I_{bit}$  is calculated by integrating the thrust  $F_x$  during one plasma acceleration over time assuming the plasma travels along the electrodes as one sheet of the thickness  $\delta$ . A summary of the derivation of  $F_x$  will be given here. For more detailed explanation see [7,8].

In the case of this thruster, the Lorentz force in  $x$ -direction, as seen in Fig. 6 is calculated by integrating over the product of the current density  $j_z$  in the plasma and the magnetic field  $B_y$  formed by the circuit:

$$F_x = m_{bit} \ddot{x} = \int_V j_z B_y dV. \quad (10)$$

This force accelerates the plasma sheet of the mass  $m_{bit}$  at a rate of change in velocity of  $\ddot{x}$ , according to Newton's law. The current density is denoted with respect to the area defined by the width  $d$  of the electrodes and the thickness  $\delta$  of the plasma sheet through which the current  $J$  passed:

$$j_z = \frac{J}{d\delta}. \quad (11)$$

The absolute current  $J$  is the value measured according to section I-C. The magnetic field  $B_y(J)$  is derived from Ampere's law. This quantity changes along the direction of  $z$  according to

$$B_y = -\frac{\mu J}{2\pi d} (\vartheta_1 + \vartheta_2). \quad (12)$$

The magnetic permeability is described by  $\mu$  and the angles  $\vartheta_1$  and  $\vartheta_2$ , indicating the position between the electrode's plates as seen in Fig. 7. This expression was obtained by integrating the magnetic field caused by every 'wire' of current passing through the electrodes over the width  $d$  of the electrode.

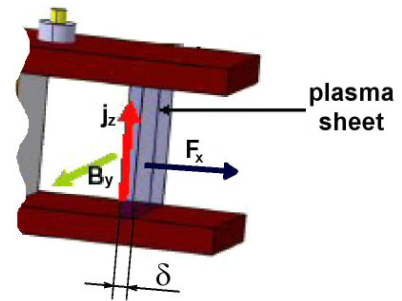


Figure 6. Current and Magnetic Field Causing Plasma Acceleration

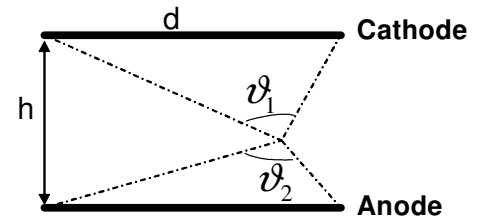


Figure 7. Angles  $\vartheta_1$  and  $\vartheta_2$

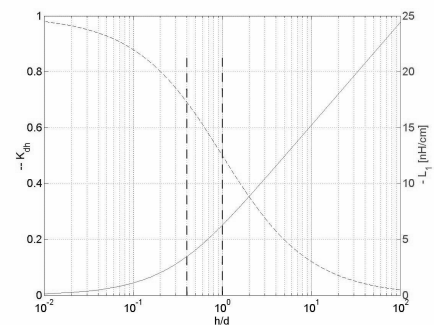


Figure 8. Correction Factor  $Kdh$  and Inductivity per Unit Length  $L1$

Inserting equations (9) and (10) in equation (8) yields for the accelerating force:

$$F_x = \frac{1}{2} \left[ \frac{\mu}{2\pi d^2} \int_0^h \int_0^d (\vartheta_1 + \vartheta_2) dy dz \right] J^2 = \frac{1}{2} L_1 J^2. \quad (13)$$

The distance between the electrodes is described by h.  $L_1$  denotes the change of inductivity per unit length passed during acceleration of the plasma. It is described by the term

$$L_1 = \mu \frac{h}{d} K_{dh} \int_{\tau} J dt, \quad (14)$$

in which  $K_{dh}$  is a correction factor, considering the ratio of h to d. This correction factor along with the resulting value for  $L_1$  can be seen in Fig. 8, along with the ratios of h/d considered for the I-MPD under discussion.  $I_{bit}$  is calculated by integrating  $F_x$  in eq. (11) over the acceleration time.

The electric efficiency  $\eta_{el}$  as derived in [7] is always greater or equal the change in inductivity from  $L_0$  to  $L_{end}$  divided by the initial inductivity  $L_0$ .  $L_{end}$  occurs when the current becomes zero and the plasma leaves the acceleration channel at  $x=x_{end}$ .

$$\eta_{el} \geq \frac{L_{end} - L_0}{L_0} = \frac{L_1 x_{end}}{L_0} \quad (15)$$

Since  $L_1$  is the change in inductivity per unit length, the efficiency is greater for higher values of  $L_1$ . Further, the specific impulse  $I_{sp}$  is calculated according to

$$I_{sp} = \frac{I_{bit}}{m_{bit} g}, \quad (16)$$

in which g is the gravitational acceleration.

An increase in  $I_{sp}$  can be produced by lowering the mass  $m_{bit}$  accelerated per pulse. It was found, that a reduction in h causes a decrease in  $m_{bit}$  [9] hence leading to the desired effect of a higher  $I_{sp}$ . However, the value of  $I_{bit}$  dropped at the same time. This is due to the fact that the ration h/d in eq. (12) was lowered, causing a decrease in  $F_x$  and in  $I_{bit}$ . To counteract this phenomena without losing  $I_{sp}$ , the width d of the electrodes was reduced. This leads to higher values for  $I_{bit}$ .

### III. Results

The results are presented for the thrust balance as well as for the effect of a change in thruster geometry.

#### A. Thrust Balance

In order to investigate the behavior of the thruster, deflection measurements were conducted varying the initial level of voltage supplied to the capacitor. In particular, the voltage was set to the levels 2200 V, 1750 V, 1650 V and 1550 V. The values for A,  $\delta$ ,  $\omega$ ,  $L_0$  and  $\Theta$  were derived from this signal for each voltage level. The data was fitted to the damped oscillation discussed in the methodology section by means of least square. Figure 9 shows the data obtained from the deflection as well as the fitted curve for a voltage level of 1750 V. A set of 5 parameters A,  $\delta$ ,  $\omega$ ,  $\alpha$  and c was obtained by performing equivalent analysis at all voltage levels investigated. Out of this set of parameters, only the amplitude A changes with the voltage level, the other parameters are not affected by higher bank energies of the thruster. All voltage levels combined, seven datasets were obtained. The change in amplitude is depicted in Fig. 10. Two and three data sets were obtained from different measurements at 1650 V and 1750 V The mean values found for the remaining parameters can be seen in Table 2 along with other characteristic values for this pendulum.

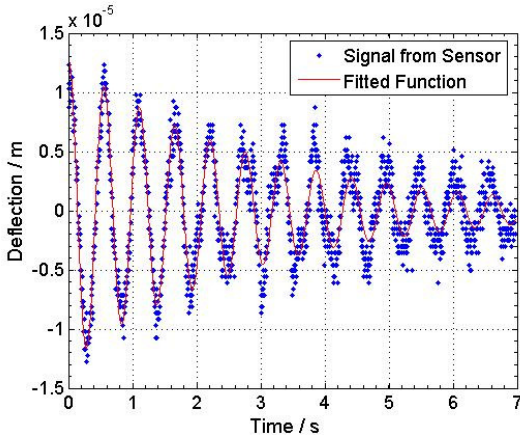


**Figure 9. Deflection Measurement of Thrust Balance over Time**

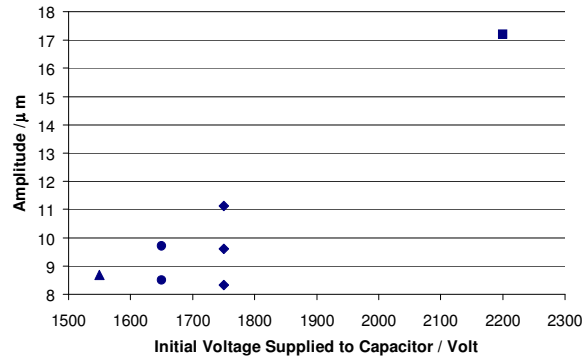


**Figure 10. Amplitude of Damped Oscillation over Initial Voltage Supplied to Thruster**

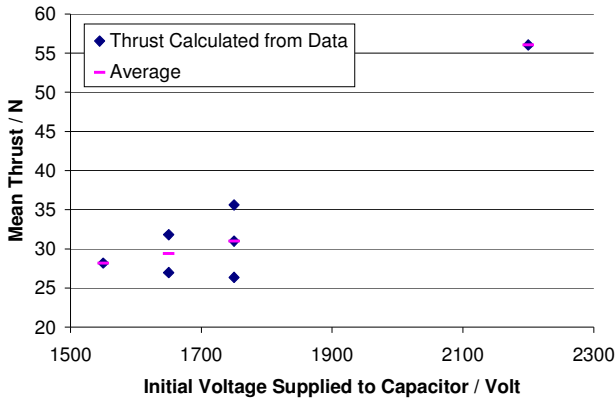


**Figure 11. Mean Thrust over Initial Voltage Supplied to Thruster**

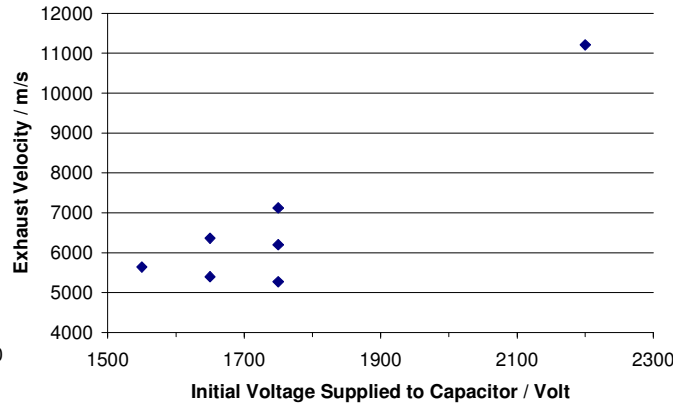


**Figure 12. Exhaust Velocity over Initial Voltage Supplied to Thruster**

Using the energy balance the mean thrust was determined according to Eq. 3, assuming an acceleration time of  $8 \mu\text{s}$  [9], as seen in Fig.11. Previous investigations [8] yielded mass bits of  $40 \mu\text{g}$  per shot at 2200 V for this distance between the electrodes. In this evaluation of the first batch of data  $40 \mu\text{g}$  was assumed for all levels of voltage. This leads to exhaust velocities of up to 11000 m/s, as seen in Fig.12. However, at this stage of investigation these results are preliminary.

During the tests, oscillation of the pendulum prior to firing the thruster was noted, even though the vibration of the turbo pump was mechanically separated from the test chamber. Active damping of the pendulum arm prior to firing the thruster, e.g. an electromagnetic solution, is necessary in this case. Further, the results presented here are based on calculation and are therefore not precise. The system will be calibrated by means of an impulse hammer, after which more precise data can be obtained.

## B. Thruster Geometry

After the variation in electrode distance was investigated in combination with the slug model [8,9], the width of the electrodes was modified in order to achieve higher thrust and efficiency levels at high levels of  $I_{sp}$ . Figure 13a and 13b show the current in the circuit over time. In both cases the maximum current is around 30 kA. The width  $d$  of the electrodes is 50 mm in Fig.13a and 40 mm in Fig. 13b. It is obvious, that the circuit with reduced width of electrodes is much more efficient. An increase in  $h/d$  lead to an optimization in efficiency as expected from eq.15.

$\delta$ [-]	0.33
$\omega$ [1/s]	11.5
$L_0$ [m]	0.274
$\theta$ [Nm $s^2$ ]	0.428
$m$ [kg]	5.71
$D$ [Nm/rad]	$2 \times 9.23\text{E-}2$

**Table 2. Pendulum Characteristics**

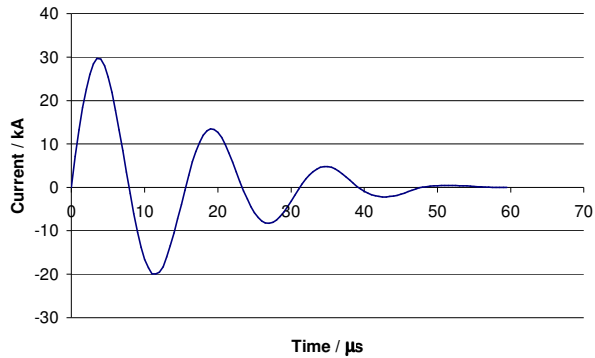


**Figure 13a. Plasma Current prior to Electrode Width Reduction**

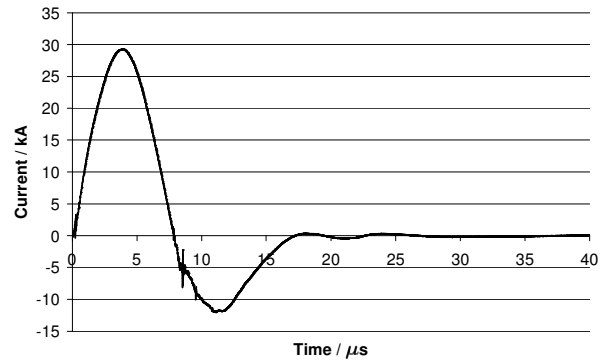


**Figure 13b. Plasma Current after Reduction of Electrode Width**

#### IV. Conclusion

The working principle of the thrust balance designed was verified. Measurements were evaluated using basic energy equations. The results obtained were in the order of magnitude expected. However, extensive calibration is being done to increase precision. Further steps include removing the igniter wires leading to the pendulum and, since the gap between pendulum and the readhead of the optical deflection sensor has to be precise, mounting the readhead on an externally controlled positioning platform.

A first step towards optimization of the geometry of SIMP-LEX was made by reducing the electrode width. The effect this caused on the behavior of the current in the circuit is favorable, and a further reduction of the width will be investigated. On the thruster side, a thorough investigation of the thermal load posed to the satellite by the I-MPD will be studied. Additionally, the propellant feeding mechanism as well as arranging the propellant needed for a lunar mission on the satellite pose a challenge.

#### Acknowledgments

The authors thank the *Deutsches Zentrum für Luft und Raumfahrt* (DLR) for their funding of this project under contract number FKZ-50-JR-0446.

#### References

- <sup>1</sup>Laufer, R. Auweter-Kurtz, M.Lengowski, M.Nawaz, A., Roeser, H.P., v. Schoenermark, M., Wagner, H., "An All Electrical Satellite for a Technology Demonstration and Science Mission to the Moon," IAC-04-Q.2b.05, 55th IAC, Vancouver, BC, 2004
- <sup>2</sup>Bock, D., Auweter-Kurtz, M., Kurtz, H., "1kW Ammonia Arcjet System Development for a Science Mission to the Moon", IEPC-2005-075, Princeton, NJ, 2005
- <sup>3</sup>R.L. Burton, Turchi, P.J., „Pulsed Plasma Thruster“, Journal of Propulsion and Power, 14/5, 716 – 735, 1998.
- <sup>4</sup>M. Hirata, H. Murakami, „Impulse Measurement of a Pulsed-Plasma Engine on Engineering Test Satellite-IV“, Journal of Spacecraft, , 21/6, 553 – 557, 1984.
- <sup>5</sup>J.R. LeDuc, D.R. Bromaghim, T. Peterson, E. Pencil, L. Arrington, W.A. Hoskins, N.J. Meckel, R.J. Cassady, „Mission Planning, Hardware Development and Ground Testing for the Pulsed Plasma Thruster (PPT) Space Demonstration on MightySat-II.1“, AIAA 97-2779, 1997
- <sup>6</sup>Antropov, N.N., Kim, V., Kozlov, V.I., Popov, G.A., Skrylnikov, A.I., "Small electric Propulsions Developed by Riame Mai", European Conference for Aerospace Sciences, EUCASS, Moscow, 4.-7. July 2005.
- <sup>7</sup>G. Jahn, R.G., "Physics of Electric Propulsion", McGraw-Hill Series in Missile And Space Technology, McGraw-Hill 1968.
- <sup>8</sup>Palumberi, S. "Initial Start-Up and Investigation of a Modular Ablative Pulsed Magnetoplasma Thruster," MS Thesis IRS-05-S-15 Stuttgart, Germany, April 2005
- <sup>9</sup>Nawaz, A., Auweter, M., Herdrich, G., Kurtz, H., "Experimental Setup of a Pulsed MPD Thruster at IRS", European Conference for Aerospace Sciences, EUCASS, Moscow, 4.-7. July 2005.